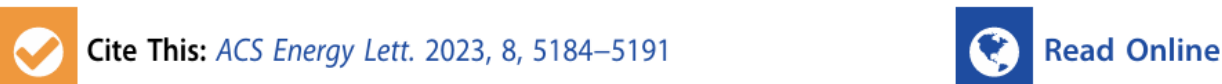


Harvesting Thermal Energy and Freshwater from Air through Sorption Thermal Battery Enabled by Polyzwitterionic Gel

He Shan, Ziya Zeng, Xinge Yang, Primož Poredoš, Jie Yu, Zhihui Chen, and Ruzhu Wang*

 Cite This: *ACS Energy Lett.* 2023, 8, 5184–5191

 Read Online

ACCESS |

 Metrics & More

 Article Recommendations

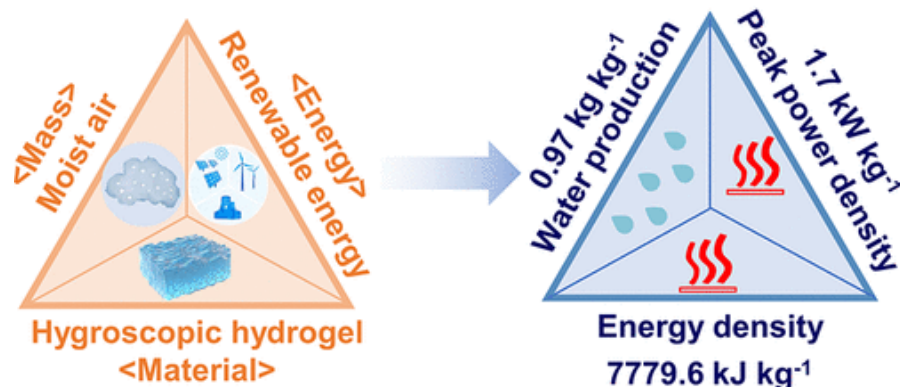
 Supporting Information

Institute of Refrigeration and Cryogenics, Shanghai Jiao Tong University, Shanghai 200240, China; Engineering Research Center of Solar Power & Refrigeration, MOE, China, Shanghai 200240, China.

Published on November 22, 2023.

Sonali Seth
January 13, 2024

Harvesting Thermal Energy and Freshwater from Air

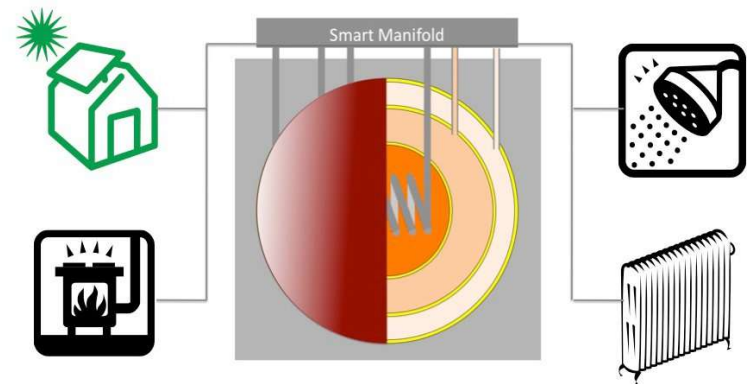


Why this paper?

A prototype has been developed that combines TES (Thermal Energy Storage) and AWH (Atmospheric Water Harvesting) technologies.

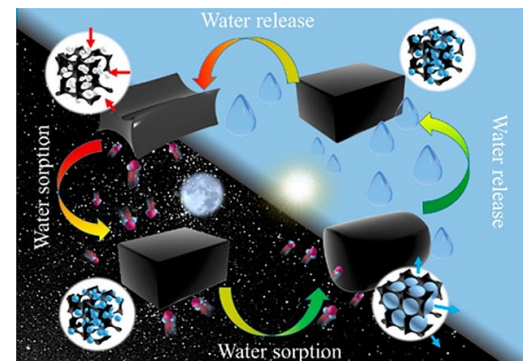
Solar Thermal batteries

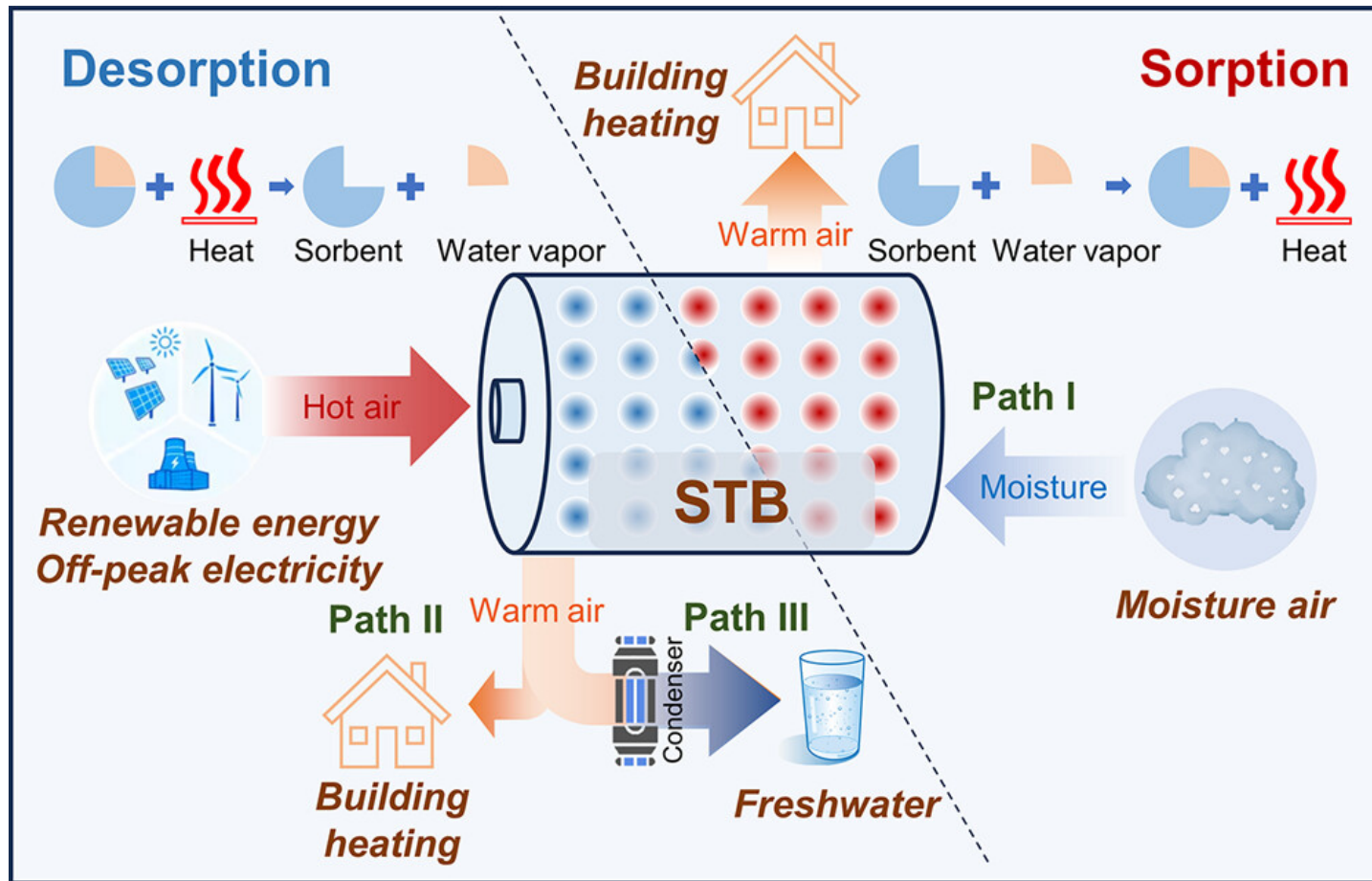
- Solar thermal batteries utilize the principle of sorption to store and release thermal energy.
- A porous adsorbent can store thermal energy in the form of latent heat and release thermal energy with high energy density.



Atmospheric water harvesting

- A porous adsorbent is used to adsorb moisture and on minimal heating, liquid water can be obtained.





Scheme 1. Three Working Paths of STB for both Thermal Energy Storage and Atmospheric Water Harvesting.

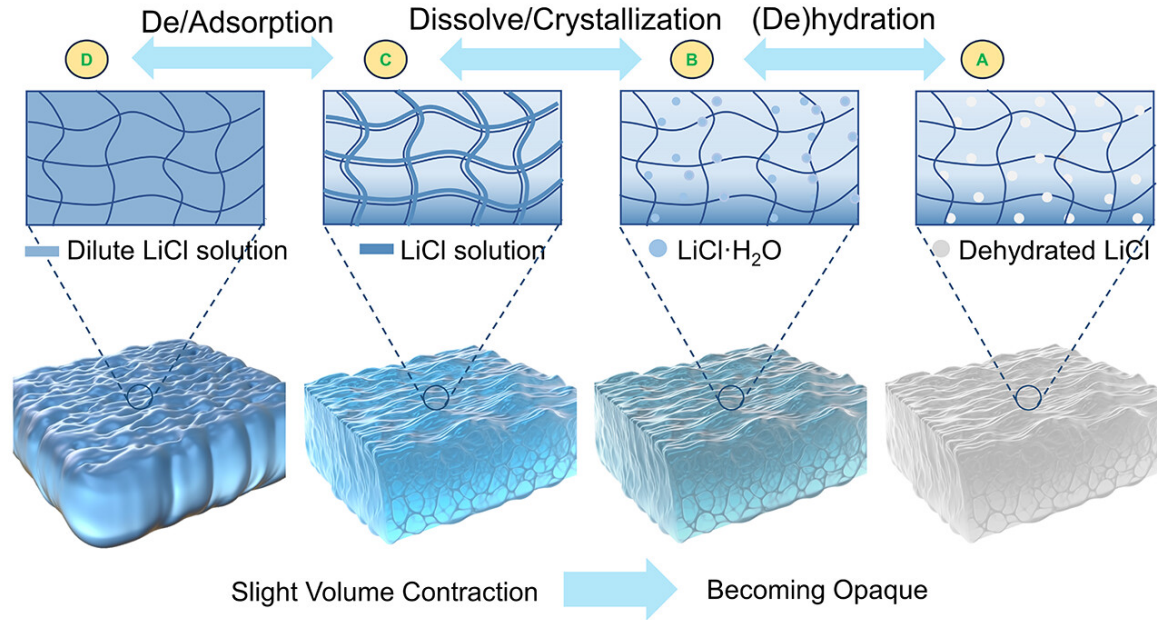
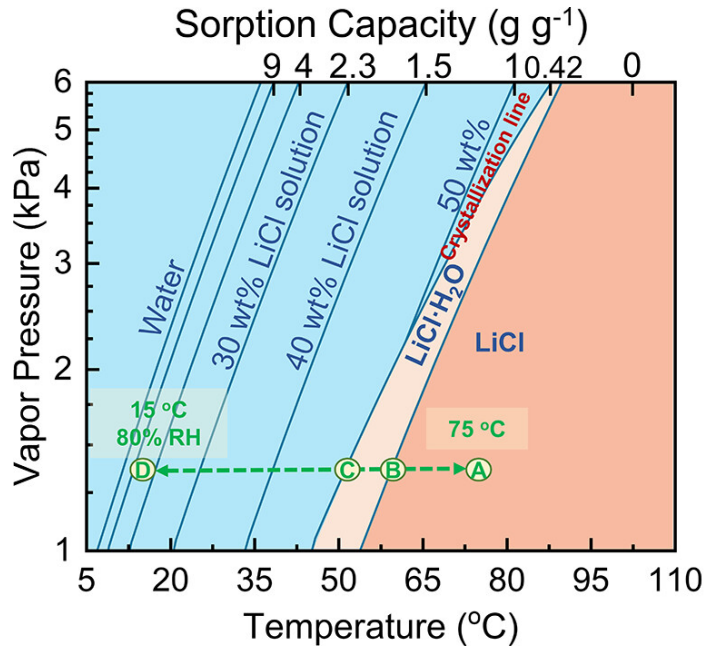


Figure 1. Vapor Pressure–Sorption Capacity–Temperature diagram, composed of vapor pressure and temperature curves for water and different concentrations of LiCl solution, along with their corresponding theoretical sorption capacities. The crystallization lines for LiCl and LiCl·H₂O are also showed. A typical open TES process is shown through the phase transition points of LiCl within the sorbent from State D to State A (Desorption) and State A to State D (Sorption). The ambient sorption condition with the temperature of 15 °C and the RH of 80% (state D) as well as the desorption temperature of 75 °C (state A) are taken as the example to show the state points.

$$\begin{aligned}
 w_{\text{gel_sorbent}} &= w_{\text{LiCl}} + w_{\text{gel_matrix}} \\
 &= x \frac{1 - \xi}{\xi} + (1 - x) w_{\text{gel_matrix}}
 \end{aligned}$$

$$\begin{aligned}
 q_{\text{gel_sorbent}} &= q_{\text{LiCl}} + q_{\text{gel_matrix}} \\
 &= x \left\{ \left(\frac{1}{\xi} - 1.42 \right) (\bar{H}_{\text{conc}} + H_{\text{water}}) \right. \\
 &\quad \left. + \frac{\bar{c}_{\text{p,sol}}}{\xi} (T_{\text{C}} - T_{\text{D}}) \right\} \\
 &\quad + 1.42x \{ \bar{H}_{\text{cr}} + \bar{c}_{\text{p,LiCl}\cdot\text{H}_2\text{O}} (T_{\text{B}} - T_{\text{C}}) \} \\
 &\quad + x \{ 1.42 \bar{H}_{\text{r}} + \bar{c}_{\text{p,LiCl}} (T_{\text{A}} - T_{\text{B}}) \} \\
 &\quad + (1 - x) \{ \bar{c}_{\text{p,gel}} (T_{\text{A}} - T_{\text{D}}) \}
 \end{aligned}$$

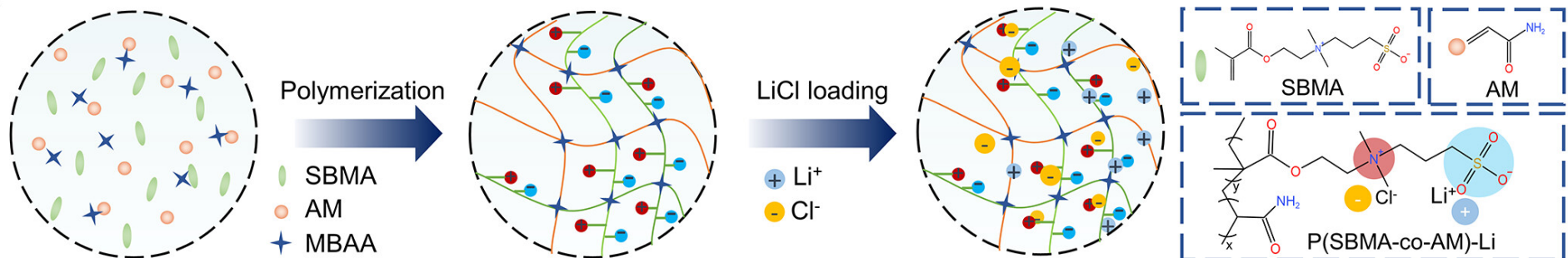
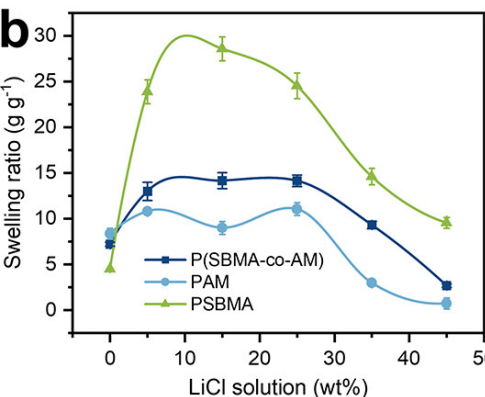
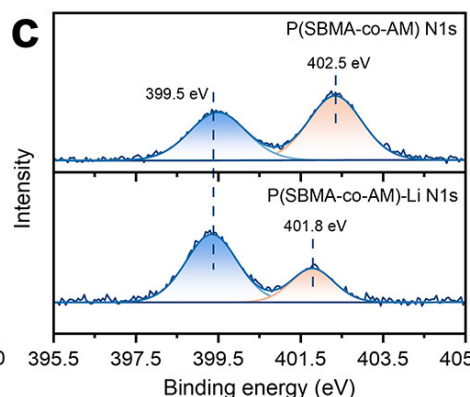
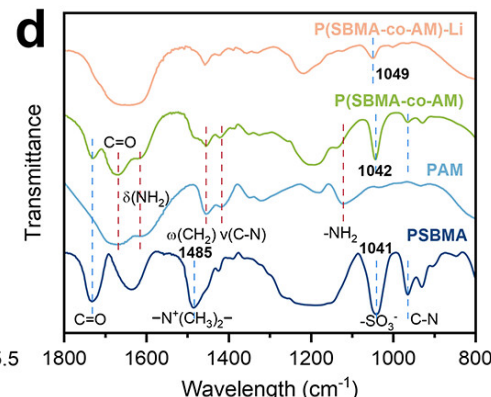
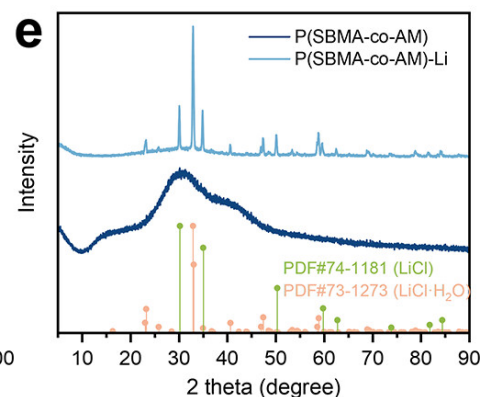
a**b****c****d****e**

Figure 2. Synthesis and characterization of P(SBMA-co-AM)-Li. a) Schematic of the synthesis process of P(SBMA-co-AM)-Li. b) Swelling ratios of PAM, PSBMA, and P(SBMA-co-AM) gel matrices immersing in deionized water and LiCl solution. c) High-resolution N 1s XPS spectra providing information on peak location and intensity shifts of the zwitterionic group. d) FTIR spectra exhibit the significant peak shift of zwitterionic groups upon coordination with salt ions. e) XRD patterns revealing the amorphous nature of the P(SBMA-co-AM) gel matrix and the sharp peaks corresponding to LiCl and LiCl·H₂O crystals in the hygroscopic gel sorbent P(SBMA-co-AM)-Li.

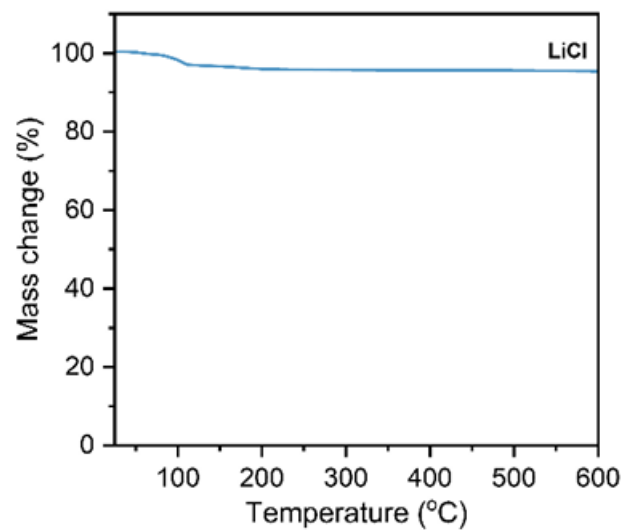


Figure S11 | TGA curve of LiCl.

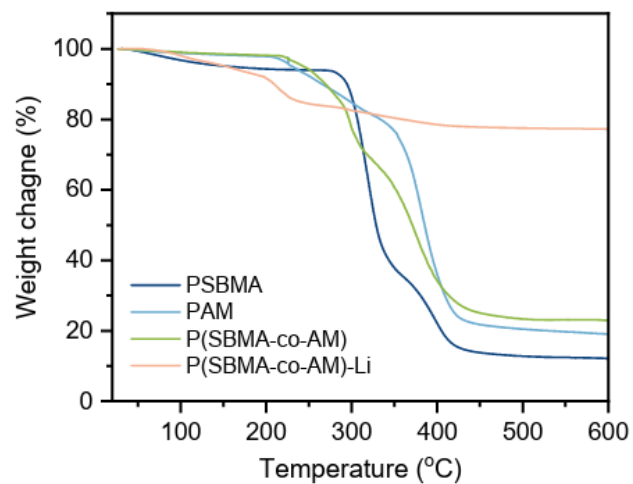


Figure S12 | TGA curves displaying the thermal stability of the PSBMA, PAM, P(SBMA-co-AM) gel, and the salt content of P(P(SBMA-co-AM)-Li gel sorbent. The salt content of the P(SBMA-co-AM)-Li gel was evaluated using TGA.

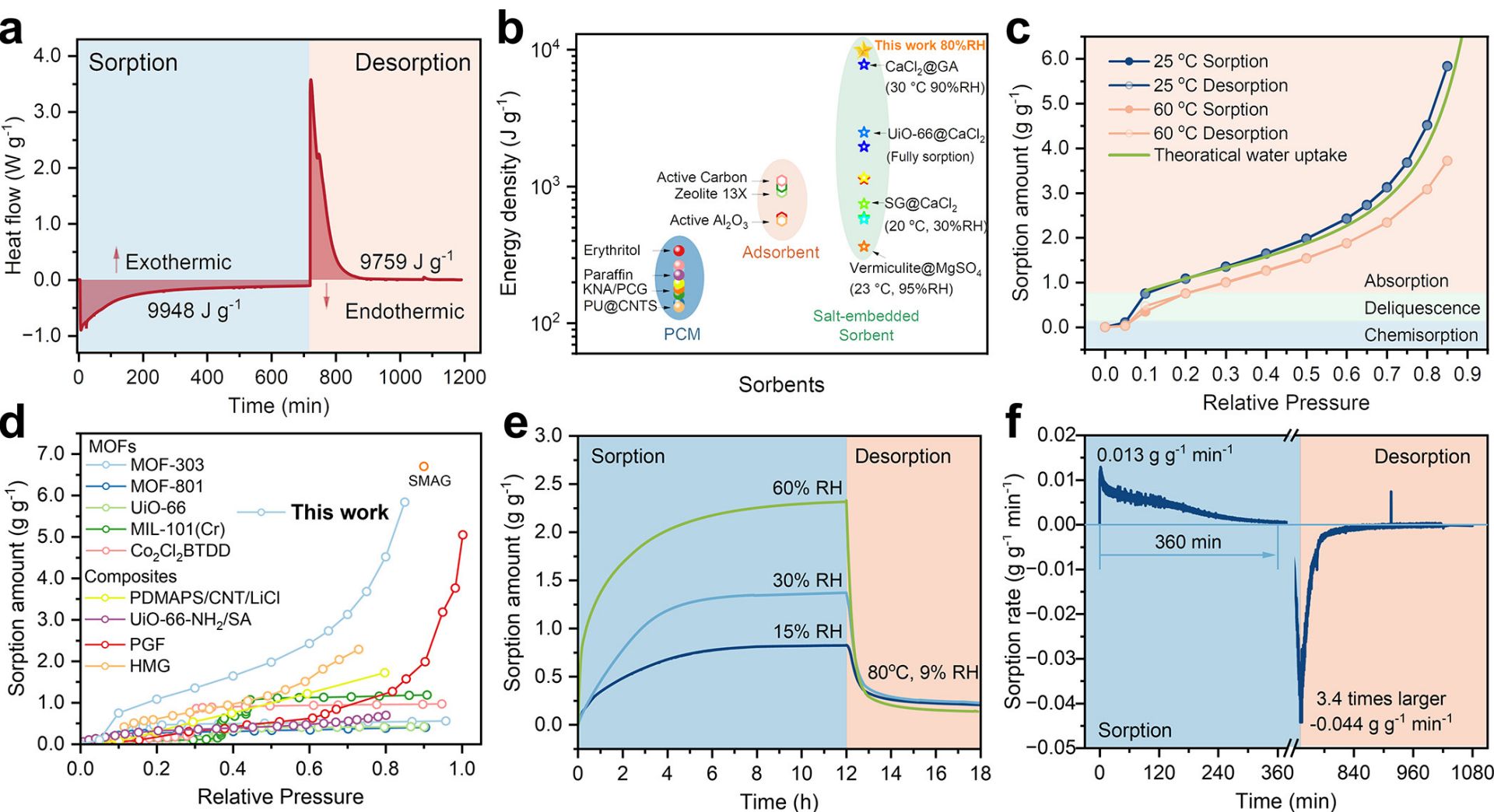


Figure 3. Water vapor sorption-desorption capacity of P(SBMA-co-AM)-Li. a) Heat flow curves obtained from the TG-DSC test for the gel sorbent during sorption at 80% RH and desorption at 60 °C. b) Energy density comparisons between P(SBMA-co-AM)-Li sorbent and previous reported PCMs, adsorbents, and salt embedded sorbents (see Table S1). c) Water sorption isotherms at 25 and 60 °C. d) Comparison of sorption capacity between P(SBMA-co-AM)-Li sorbent and previous reported MOFs, gels, and composite gels. e) DVS curves display dynamic water sorption-desorption processes. f) Derivative sorption amount changes of the milligram-scale sample at 30% RH.

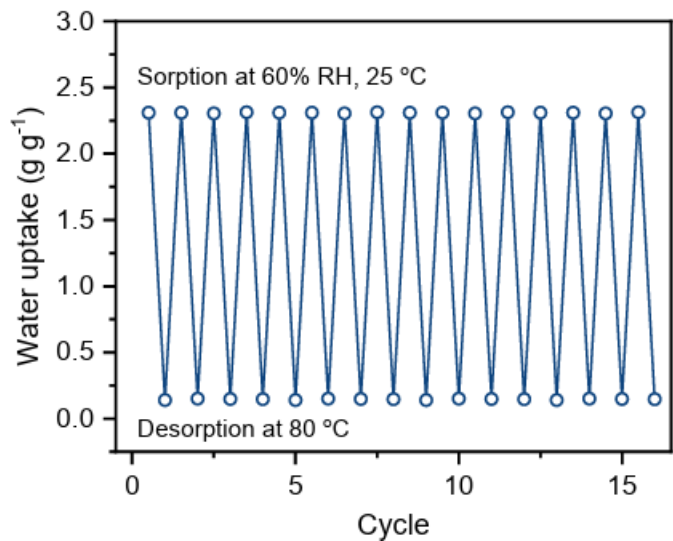


Figure S18 | Fifteen water sorption-desorption cycling tests carried out at 25°C, 60% RH for sorption and 80°C for desorption, indicating satisfactory water sorption-desorption cycling stability

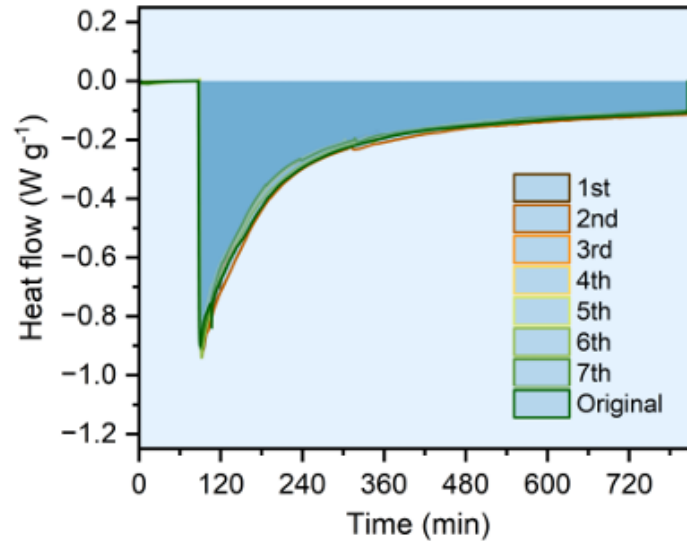
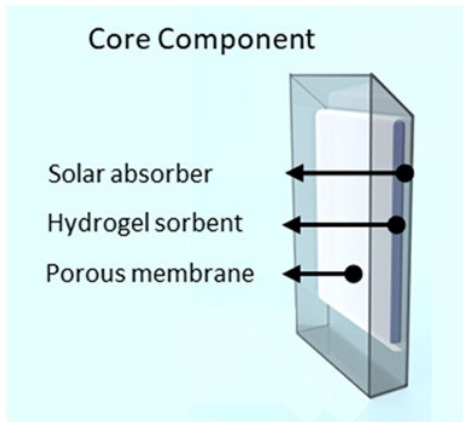


Figure S19 | Heat flow curves during 7 adsorption-drying cycles of the same sample. It is evident that not only the heat release but also the heat release rate remains consistent, confirming the stability of the thermal storage performance during the cycling process. We have also included the results from earlier sample batches, demonstrating uniformity across different sample batches.



The core components of the decoupled device include a solar absorber, a gel sorbent, and a porous membrane.

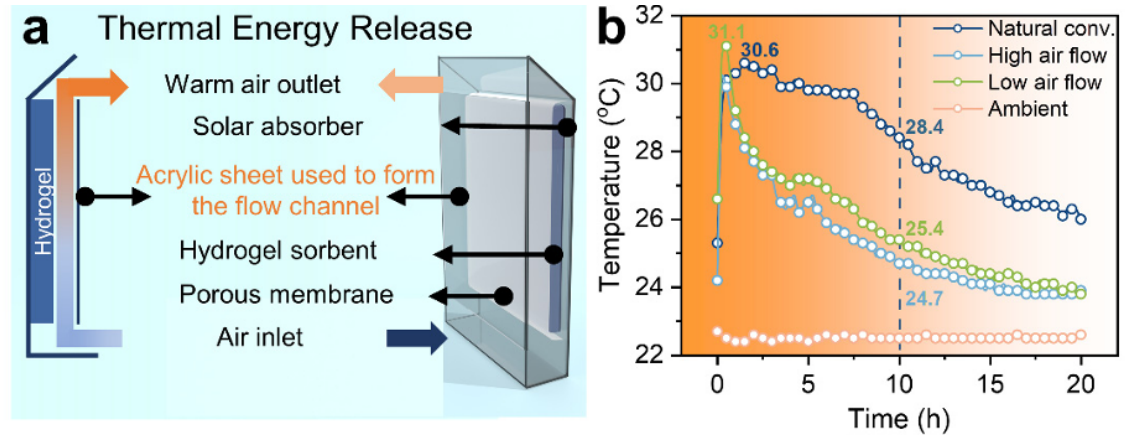


Figure S33 | Heat release mode of the solar-driven single-function devices for ATB and AWH. (a) Thermal energy release mode of the single-functional device. (b) The variation in output air temperature under various air flow rates.

Heat Storage Mode

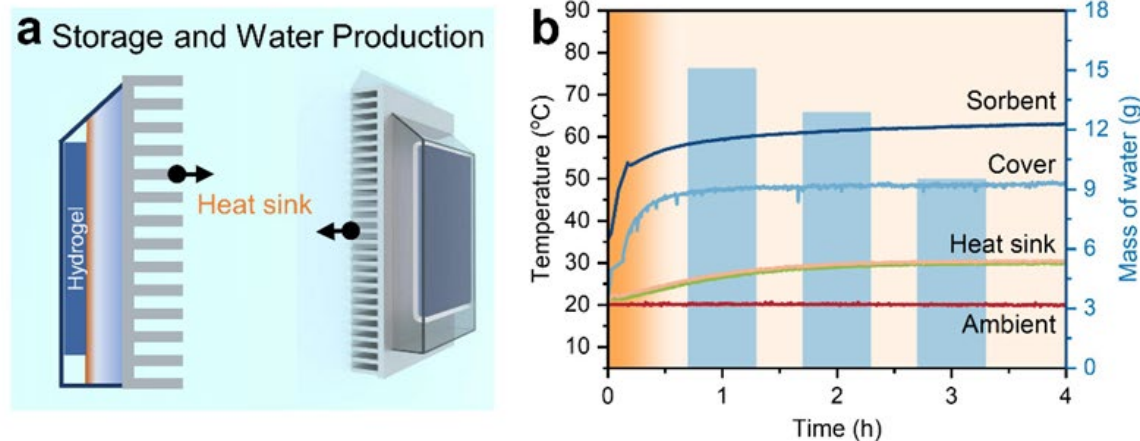


Figure S34 | Heat storage mode of the solar-driven single-function devices for ATB and AWH. (a) Energy storage and water production mode of the single functional device. An aluminum heat sink is used to create an enclosed wall and a heat dissipation channel. (b) Temperature profiles of the various components during the energy storage mode. and Water capture, release, and acquisition during the water harvesting process.

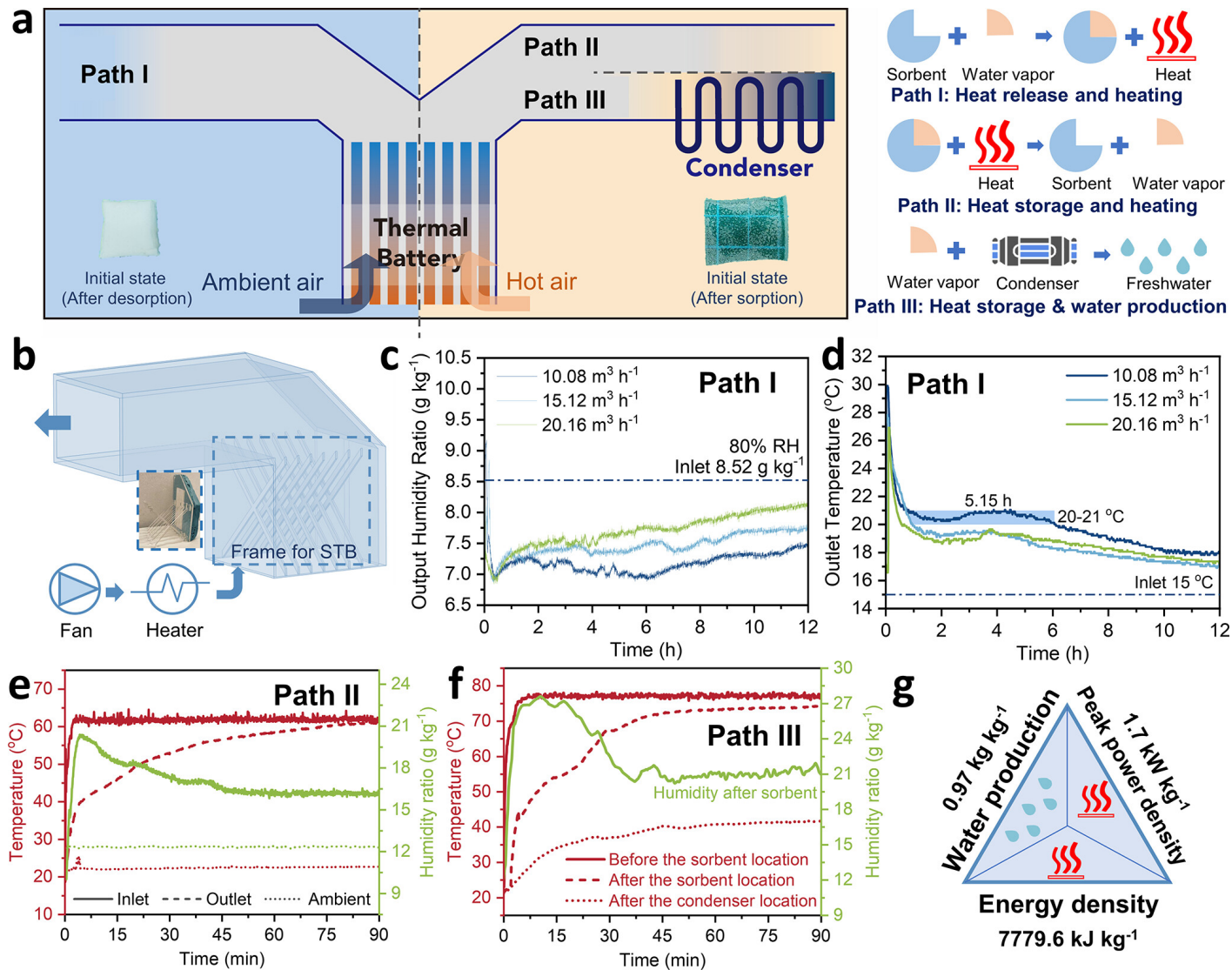


Figure 4. Device and experimental results for achieving dual-functional STB and AWH. a) The flow schematic and three working paths of the device for thermal release, TES, and AWH. b) The schematic diagram of the lab-scale demonstration device and the supporting frame for the STB. c) The humidity variation at the heat release mode (Path I) driven by various airflow rates, as well as d) the corresponding output temperature variation. e) Temperature and relative humidity variation at the heat storage path (Path II) under an input temperature of 61 $^{\circ}\text{C}$. f) Temperature and relative humidity changes at the water production path (Path III). g) Schematic summarizing performance metrics in the three paths, including water production, peak power density, and energy density.

Conclusion

- A prototype is designed to couple AWH and TES.
- Adsorbent exhibits a high sorption enthalpy of 9948 KJ/Kg and significant sorption from 1.07 g/g to 5.82 g/g over a RH range of 20% to 85%.
- The designed integrated device demonstrates effective thermal energy collection and storage, achieving an energy density of 7779.6 kJ/kg , a peak power density of 1.7 kW/kg , and a water productivity of 0.97 kg/kg